Evaluation of the Flow Quality in the MTL Wind-Tunnel

by

Björn Lindgren & Arne V. Johansson

Department of Mechanics

October 2002
Technical Reports from
Royal Institute of Technology
Department of Mechanics
SE-100 44 Stockholm, Sweden

Typsatt i $\mathcal{AMS}$-LaTeX med Osos *rapport*-stil.

Universitetsservice US AB, Stockholm 2002

Contents

1. Introduction 1
2. Experimental setup 7
3. Results 12
4. Concluding remarks 29
5. Acknowledgment 30

References 30

Appendix 33

Evaluation of the flow quality in the MTL wind-tunnel

By Björn Lindgren and Arne V. Johansson

Dept. of Mechanics, KTH, SE-100 44 Stockholm, Sweden

Technical report. TRITA-MEK 2002:13

The flow characteristics of the MTL wind-tunnel at the Department of Mechanics, KTH, have been evaluated 10 years after its completion. The wind-tunnel is of closed circuit type with a 7 m long test section that has a cross section area of 1.2×0.8 m^2. The contraction ratio is 9 and the maximum speed is approximately 70 m/s. The experiments performed included measurements of total pressure variation, temperature variation, flow angle variation and turbulence intensity variation. The measurements were carried out in the test section over a cross flow measurement area of 0.9×0.5 m^2 located 0.4 m downstream the inlet. The temperature variation in time was also measured at the center of the measurement area. The experiments were performed at three different wind-tunnel speeds, 10, 25 and 40 m/s. The present results confirm that the high flow quality of the MTL wind-tunnel. The flow quality measurements carried out soon after the completion of the tunnel are here repeated and extended. For instance, at 25 m/s the streamwise turbulence intensity is less than 0.025% and both the cross flow turbulence intensities are less than 0.035% at the same speed. The total pressure variation is less than ± 0.06% and the temperature variation is less than ± 0.05 °C.

1. Introduction

The Minimum Turbulence Level or Mårten Theodore Landahl (MTL), wind-tunnel, named after its late initiator, was designed in the mid 80s to suit experiments in basic transition and turbulence research. The wind-tunnel that was completed in 1991 has now been in operation for 10 years and it was decided to re-confirm the early flow quality measurements and to extend them with the aid of the accurate and automated traversing equipment now in use. The French company Sessia was contracted for the wind-tunnel construction, although the responsibility for the aerodynamic design remained with the Department of Mechanics. The primary aim of the early tunnel calibration study was to perform experiments that could confirm that the design requirements in the contract were fulfilled. The main results were reported in Johansson (1992).

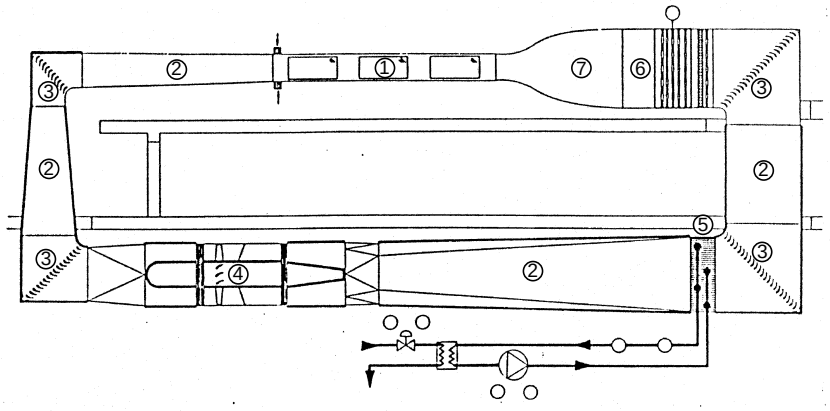

FIGURE 1. The MTL wind-tunnel layout.

At that time no automated traversing system existed and the manual system used only allowed for measurements coarse spatial resolution. In experiments similar to those in the early study have been performed allowing for direct comparisons. This is important not just from the point of view of establishing the current status of the flow quality but also to analyze the effect of the wear on the wind-tunnel parts. It is commonly known that *e.g* the maximum speed of a wind-tunnel is usually decreasing with time but is there also a negative effect on the flow quality from possible deterioration of screens, honeycomb and machinery? Answering questions like these helps planning for future maintenance of the wind-tunnel circuit.

In the MTL wind-tunnel many landmark experiments have been performed over the years. A complete list of the doctoral and licentiate thesis where the MTL wind-tunnel was used is given in appendix 5 together with a short description of the main findings in these works. Other landmark papers with measurements performed in the MTL wind-tunnel are also described and listed in the appendix.

1.1. *Description of the MTL wind-tunnel*

The MTL wind-tunnel is a closed loop circuit wind-tunnel. The advantages of a closed loop tunnel is that less energy is needed to operate the tunnel at a given speed and that disturbances in the tunnel surroundings do not interfere with the flow inside the tunnel making it easier to control the mean flow characteristics during measurements. A small gap between the test section and the first diffuser ensures that the static pressure in the test section is close to the

atmospheric pressure. The overall length of the MTL tunnel is about 25 m and the height is 9 m.

Its design is optimized for very good flow quality rather than low total pressure drop, see Johansson (1992). The efficiency factor, λ, is a measure of the losses in the wind-tunnel circuit, defined as

$$\lambda = \frac{\Delta p_{\mathrm{tot}}}{q_{\mathrm{test}} \eta_{\mathrm{fan}}}, \tag{1}$$

where Δp_{tot} is the total pressure-loss, q_{test} is the dynamic pressure in the test section and η_{fan} is the efficiency factor of the fan. For the MTL tunnel the efficiency factor is about 0.4. In figure 1 a side view of the tunnel circuit is presented with the numbers referring to different parts of the wind-tunnel.

1.1.1. *Test section*

The test section, item ① in figure 1, is 7 m long and it has a cross section area of 1.2×0.8 m^2 (at the inlet). The dimensions of the test section ensures that *e.g.* experiments on a flat plate at fairly high Reynolds numbers can be achieved without a very high free stream velocity, see *e.g.* Österlund & Johansson (1999). The cross section area is large enough to enable measurements at the downstream end of the test section without interference from the test section wall boundary layers. The top and bottom walls are adjustable so that the streamwise pressure gradient can be modified between moderate negative to moderate positive values. Most importantly, a zero streamwise pressure gradient can be achieved by compensating for the boundary layer growth on the test section walls. This can be achieved to within a variation of 0.2% of the free stream velocity, see Österlund (1999). A traversing arm penetrates the top wall of the test section. The traversing system has 5-axes making it possible for a measurement probe to be translated in the three spatial directions and to be rotated along the streamwise axis and along one cross flow axis free of choice. An extra long sting facilitates measurements in the contraction, see Sjögren & Johansson (1998). The maximum free-stream velocity in the (empty) test section is approximately 69 m/s.

1.1.2. *Diffusers*

The diffusers, items ② in figure 1, are conservatively designed so that wall boundary layer separation is avoided at any time, see *e.g.* Seidel (1982). For very large flow disturbances, vortex generators, see *e.g.* Lin *et al.* (1991), can be mounted in the first diffuser downstream of the test section. Calculations have been made to find the optimum shape of the diffuser downstream the fan. The calculations combined the potential theory with boundary layer equations. Model experiments were also performed using a 2 m long diffuser. Various shapes and inlet conditions were investigated to achieve an efficient

diffuser without wall boundary layer separation. The conservative design of the diffusers leads to a longer wind-tunnel return circuit and is one contributing factor to the relatively large total pressure-loss in this wind-tunnel circuit compared to wind-tunnels used for commercial testing.

1.1.3. *Corners*

One wind tunnel part that could cause flow disturbances, and especially noise is the corner, item ③ in figure 1. The corner, which turns the flow 90°, are equipped with a cascade of airfoils, here called guide-vanes. If the guide-vanes are not properly designed they could be exposed to large boundary layer separations leading to poor flow uniformity, large turbulence levels as well as high total pressure-loss. In the design of the MTL tunnel, special care was given to this detail with experiments and calculations performed by Sahlin & Johansson (1991). In addition to the published results for profiles with turbulent boundary layers, a very efficient guide-vane with laminar boundary layers and a two-dimensional total guide-vane pressure-loss coefficient as low as 0.036, measured at the first corner downstream the test section, was designed for use in the MTL-tunnel. Despite the very low pressure-loss the guide-vanes allows for moderate ($\pm 2°$) changes in angle of attack without separating. It is important to design a guide-vane that will perform well under adverse flow conditions especially in the first corner where measurement equipment may disturb the flow substantially.

1.1.4. *Driving unit*

Item ④ in figure 1 is the fan and motor. The fan used in the MTL tunnel is of axial type with 12 blades and the motor mounted directly onto the fan axis. The motor is of DC current type and it is enclosed in a cylinder with the same diameter as the fan hub for reasons of improved aerodynamics. It is cooled separately by a fan outside the tunnel circuit and cooling air is supplied to the enclosed cylinder through elliptical pipes. This means that the heat generated by losses in the motor does not need to be removed by the wind-tunnel heat exchanger. The power of the motor is 85 kW and the speed of the fan is controlled by a thyristor control unit.

In-front of and behind the fan there are silencers with central bodies to minimize noise disturbances from the fan. The upstream central body has the diameter of the fan hub and an ellipsoidal shaped nose cone. The central body of the downstream silencer is shaped as a cone with the base diameter equaling the upstream central body diameter. The upstream silencer also converts the tunnel circuit cross section from square to circular and the downstream silencer converts the cross section from circular to octagonal shape, which is the shape of the following diffuser, see figure 1. The walls of the silencers and their central bodies are made of perforated plates with a thick sound absorbing material (long fibered glass-wool covered by a woven glass-fiber material) for good

efficiency. The wind-tunnel parts located between the first and forth corners have sound insulated walls, resulting in a very quiet wind-tunnel. Measurement of the noise level inside the test section was performed and are reported in Johansson (1992).

1.1.5. *Heat exchanger*

The tunnel circuit heat exchanger, item ⑤ in figure 1, is located at the lower part of the wind-tunnel just in-front of the third corner counting from the test section in the downstream direction. This positioning of the heat exchanger is conservative in some sense of ensuring that the temperature variation in the test section cross section is small. A small drawback of this positioning is that the cross section area is slightly higher here than in the stagnation chamber, see 1.1.6, leading to a small increase in local pressure drop.

The tubes of the heat exchanger are of elliptical cross section shape which decreases the local pressure drop slightly compared to standard circular pipes. Cooling flanges are mounted onto the pipes to increase the cooling area of the heat exchanger. Extra turbulence generators can also be added to the cooling flanges to enhance the heat transfer, but such items are not used here because of the very high pressure drop and the increase of the turbulence level caused by these turbulence generators.

The water flowing through the heat exchanger has a high and constant flow rate. It is cooled through an additional heat exchanger by water from an external, in-house, cooling system. A valve regulates the flow rate in the external system thereby controlling the temperature of the water passing through the wind-tunnel heat exchanger. This valve is regulated by a commercial PID regulator.

The temperature in the wind-tunnel test section is measured by a PT-100 sensor and is used as input into the PID regulator. The set, (chosen), wind-tunnel temperature is entered manually from the regulator front panel.

1.1.6. *Stagnation chamber*

The stagnation chamber, or settling chamber as it is often called, item ⑥ in figure 1, has the largest cross section area, and thereby also the lowest flow velocity, in the wind tunnel circuit. This is where items used for flow quality improvements are located such as screens and honeycomb. Sometimes the heat exchanger is also located here, see *e.g.* Seidel (1982), to minimize the local pressure-drop. This positioning was here rejected because of the ambition to achieve a high degree of temperature uniformity in the test section.

The MTL stagnation chamber consists of three different parts, the honeycomb, the screens and the relaxation duct, in that order of location relative to the flow direction.

The purpose of the honeycomb is to break up large eddies into smaller ones and, more importantly, to rectify the flow coming from the fourth corner. A screen also rectifies the flow to some extent but the honeycomb is more efficient in this respect and it has a lower cost in pressure drop. The ratio between the length, (in the streamwise direction), and the cell diameter of the honeycomb is the most important parameter influencing the degree of flow rectification, see *e.g.* Lumley (1964); Loehrke & Nagib (1976); Scheiman & Brooks (1981). The honeycomb is 100 mm long and the cell diameter is about 10 mm in the MTL tunnel.

The screens on the other hand are more efficient than the honeycomb in reducing the turbulence by breaking down larger eddies into smaller ones with a size of the mesh width, see *e.g.* Laws & Livesey (1978) and Groth & Johansson (1988). The screens are also very effective in reducing mean flow variations over the cross section area. This ability is related to the solidity, *i.e.* the ratio of blockage generated by the screen wire front area, and the pressure drop coefficient of the screens, see Taylor & Batchelor (1949). It has been found that a combination of screens with decreasing mesh sizes in the downstream direction is very efficient in reducing mean flow variations, see *e.g.* Groth & Johansson (1988). The distance between the screens has to be more than about 30 mesh sizes to let the screen wire induced turbulence die out sufficiently before it hits the next screen. The porosity of the screens must also be larger than about 55% to avoid a phenomenon called jet collapse, see Baines & Peterson (1951). Jet collapse leads to a strong mean flow variation and must be avoided. In the MTL tunnel there are 5 screens with decreasing mesh size in the streamwise direction between 3.1 mm and 0.75 mm. These values were chosen carefully after a study made by Groth & Johansson (1988) for maximum screen efficiency.

The effect of turbulence reduction of the screens is much larger in the streamwise component than in the cross stream components of the flow. This is especially true for under-critical screens where up to 90% of the reduction is in the streamwise component, see Groth & Johansson (1988); Tan-Atichat *et al.* (1982). This means that the flow is very non-isotropic just downstream of the screens making it important to allow the flow to relax towards a state of isotropy before it enters the contraction where it again will be subjected to high strains. This is achieved at the downstream end of the non-diverging stagnation chamber. The length of this section is 750 mm in the MTL tunnel, which is a long enough distance for the flow to reach an approximately isotropic state.

1.1.7. *Contraction*

The final part in the wind-tunnel return circuit is the contraction, item ⑦ in figure 1. It transform the wind-tunnel cross section area back to that of the test section. The contraction also reduces the relative mean flow velocity variation and turbulence intensity. These reductions are much larger in the streamwise

direction than in the cross stream directions. They are also highly dependent on the contraction ratio with increased reduction for increasing contraction ratio, see *e.g.* Johansson & Alfredsson (1988). The contraction ratio in the MTL tunnel is 9, *i.e.* the area ratio between the stagnation chamber and test section cross section areas. This value is rather high compared to most other wind-tunnels but there are occasional examples of even higher contraction ratios. The drawback of a high contraction ratio is the relative increase in tunnel return circuit length, highly non-isotropic flow in the test section inlet and an increased risk for separating boundary layers on the contraction walls.

The shape of the contraction has to be designed very carefully to avoid wall boundary layer separation. A contraction can be divided into one upstream concave part and one downstream convex part. Separation can occur in both these parts. A boundary layer separation is induced by a positive pressure gradient along the contraction wall and is caused by the curvature of the wall. It is present even though the mean flow in general is accelerating due to the decrease in cross section area. Positive pressure gradients are found both in the concave part close to the inflection point, where the shape of the walls become convex, and at the downstream end of the convex part. A separation occurring in the concave part is very difficult to eliminate once the contraction is built which means that it has to be avoided already at the design stage. A separation bubble in the convex part, however, can be eliminated by tripping the laminar boundary layer achieving transition to a turbulent boundary layer that is more resistant to separation. This kind of boundary layer tripping is implemented in the MTL tunnel using V-shaped dymo-tape as roughness elements.

The shape of the contraction used in the MTL wind-tunnel was optimized using flow calculations. These calculations were based on a combination of potential theory and boundary layer equations. They were performed using a code that was provided by Downie *et al.* (1984). The aim was to minimize the contraction length keeping a wall pressure gradient distribution without risk for wall boundary layer separation. For further information on optimization of three dimensional wind-tunnel contractions see *e.g.* Borger (1976); Mikhail & Rainbird (1978).

The final shape chosen for the MTL-tunnel can be expressed as a combination of sinus-hyperbolic functions where the concave part covers the first 70% of the contraction length and the convex part the remaining 30%.

2. Experimental setup

The present measurements were performed in a cross section of the test section at a position 400 mm downstream the test section entry. The area covered by the measurement probes was 900×500 mm^2 and located around the center, see figure 2. This area is here referred to as the measurement region. The area ratio between the measurement region and the test section is 0.47, thus almost half the total area is covered in the experiments. The reason for excluding the

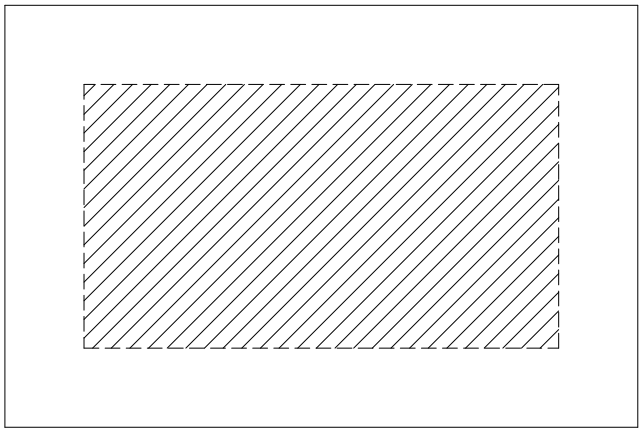

FIGURE 2. The cross section of the test section. The hatched area is the area covered in the measurements.

150 mm wide rim closest to the walls is that the flow is here disturbed by the tunnel circuit walls and it is usually not included when figures of wind-tunnel flow qualities are compared. The velocity variation is stronger in the rim than in the core region (measurement region). Therefore most experiments occurring in the MTL tunnel are performed in the core region. Also by excluding the rim the calibration range of the probes can be minimized increasing the resolution of the measurements in the core region. The measurements were performed at three different test section free stream velocities covering a large part of the wind-tunnel velocity range. The three velocities are 10 m/s, 25 m/s, and 40 m/s. These velocities were chosen because they are representative for many of the experiments performed so far in the MTL tunnel. 10 m/s is a typical velocity for experiments on transition phenomena, 25 m/s is a typical velocity for medium Reynolds number experiments and 40 m/s is a typical velocity for higher Reynolds number experiments. The fan blade angles are not easily changed and they are positioned for maximum performance at around 25 m/s. Therefore we expect the results of these measurements to be most favourable at 25 m/s free-stream velocity.

The traversing system used is a 5-axes system, see section 1.1.4. This system can traverse a probe in the streamwise and cross stream directions. It can rotate the probe around its own axis and it can also change the angle of attack. The last feature makes it possible to calibrate a cross wire probe or a flow angle probe without removing them from the test section, making the calibration more accurate. The traversing system and the wind-tunnel velocity are controlled from a computer.

2.1. *Measurement instrumentation*

For the hot-wire measurements we used a two-channel anemometer, (AN-1003), from AA Labs (Israel). For further amplification of the hot-wire signal a stereo amplifier, (AX-490), from Yamaha was used. This amplifier was also used to filter the signal, removing contributions from noise at very high frequencies. The signal was then sampled into a computer by a 12 bit AD board.

The measurement of the dynamic pressure was achieved through a differential pressure transducer, (FCO510) from Furness Control, (Great Britain). The absolute accuracy of the pressure transducer is 0.25% of full scale, ($\pm$2000 Pa). The sampled data are transfered to the measurement computer through the serial bus.

The temperatures were measured using Pt-100 sensors. The absolute accuracy of these sensors is in the order of 0.056 °C per °C. A 6 digit accurate multimeter (HP-34401A) from Hewlett Packard with a built in 4-wire compensation resistance meter was used to measure the probe resistance. The 4-wire compensation eliminates any contribution from the inherent resistance in the connecting cables. The measured data was then transferred to the measurement computer through GPIB communication and then converted into temperatures using the following equation

$$R_{\mathrm{t}} = R_0 \left(1 + AT + BT^2\right), \tag{2}$$

where R_{t} is the probe resistance, R_0 is the resistance at 0°C, T is the temperature and A and B are constants.

2.2. *Probe calibrations*

The probes used were single- and cross- hot-wire probes and a flow angle probe. Calibrations of the hot-wire probes were performed immediately before every new measurement. The flow angle probe was calibrated using several runs to verify the calibration accuracy.

2.2.1. *Single-wire probe calibration*

The exclusion of the near wall region allows the velocity range over which the calibration is made to be very small. This means that the calibration can be made with high accurately. The error in streamwise velocity for the single-wire calibrations was less than $\pm$0.05%. The single wire was calibrated in the free stream using King's law

$$U_0 = \left(\frac{E^2 - A}{B}\right)^{\frac{1}{n}} \tag{3}$$

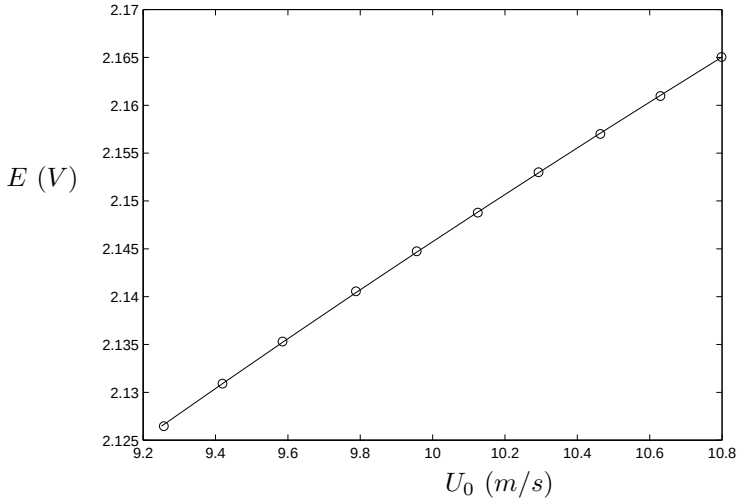

FIGURE 3. A typical calibration of a single-wire. The circles are measured points and the solid line is the King's law derived by a least square fit to the measured points.

where U_0 is the free-stream velocity, A, B and n are constants to be determined and E is the voltage output from the anemometer. The mean velocity, U_0, was determined through the relationship

$$p_{\text{tot}} - p = \frac{1}{2}\rho U_0^2 \tag{4}$$

using a Prandtl tube to measure the dynamic pressure. The density and viscosity of the air could be determined accurately by measuring the static pressure and the temperature. In equation 4, p_{tot} is the total pressure, p is the static pressure and ρ is the air density. A typical single-wire calibration curve is seen in figure 3.

2.2.2. *Cross-wire probe calibration*

Calibrating the cross-wire probe includes variations both in the velocity and probe angle of attack. A surface is then fitted to the measured data points using a fifth order polynomial. The use of a polynomial that lacks any relevant physical information makes it extra important not to allow any data points outside the calibration range during measurements. This may lead to strongly erroneous results.

The streamwise and cross stream velocities were determined by the equations

$$U = U_0 \cos\alpha, \tag{5}$$
$$V = U_0 \sin\alpha, \tag{6}$$

where U and V are the streamwise and cross stream velocity components respectively and α is the probe angle of attack. Two help variables, x and y representing the streamwise and the cross stream velocity components, are calculated from the wire voltages E_1 and E_2 as follows

$$x = E_1 + E_2, \tag{7}$$
$$y = E_1 - E_2, \tag{8}$$

These variables are then used to construct two two-dimensional fifth order polynomials, here denoted by M and N, for the two variables, U and $\tan\alpha$. By solving the following equations in a least square sense

$$MA = U, \tag{9}$$
$$NB = \tan\alpha, \tag{10}$$

the coefficients in the vectors A and B can be determined. These coefficients are then stored and used later in the experiments to determine the instantaneous velocities, u and v.

In figure 4 the results from a typical cross-wire calibration is shown. The area inside the solid lines is the calibration area where all measurement points must lie. The error of the cross-wire calibration was less than $\pm 0.05\%$ for the streamwise, U, component and the cross stream components V and W.

2.2.3. *Flow angle probe calibration*

The flow angle probe was calibrated by altering the probe angle of attack in the center of the measurement area. The shape of the probe makes it very sensitive to flow angle variations. There are two pressure holes, one on each side of the probe close the bottom of the V-shaped cut, see figure 5. When the stagnation point at the bottom of the V cut moves towards one side a pressure difference can be measured between the holes. The inclined edges of the V cut accentuates this pressure difference. The pressure difference is measured for different angles of attack and a least square fit of a third order polynomial is then made to the measured data points. In figure 6 a typical calibration of a flow angle probe is shown. The error in the flow angle calibrations is less than $\pm 0.02°$.

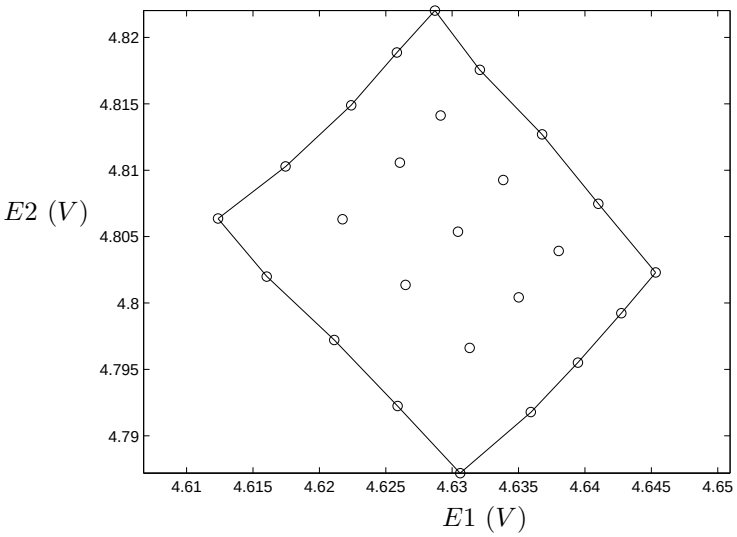

FIGURE 4. A typical calibration of a cross-wire. The circles are measured points and the solid lines represent the border of the calibration area.

FIGURE 5. The flow angle probe. The horizontal direction is sensitive to flow angle of attack.

3. Results

In this section we will present results for some important measures of flow quality. The quantities presented are, in order of appearance, the total pressure variation, which is a measure of the streamwise flow uniformity over the measurement area, the temperature variation, the flow angularity, which is a measure of how parallel the flow is and the turbulence intensities in both the streamwise and the two cross stream directions.

The measurement area (900×500 mm^2) leaves out a rim of 150 mm along the test section walls where the flow is affected by the proximity of the walls. The streamwise position of the measurements is 400 mm downstream of the test section inlet. This position was chosen because it is far enough upstream to minimize disturbances from the test section walls and far enough downstream to allow the flow to relax after the high strain encountered in the contraction.

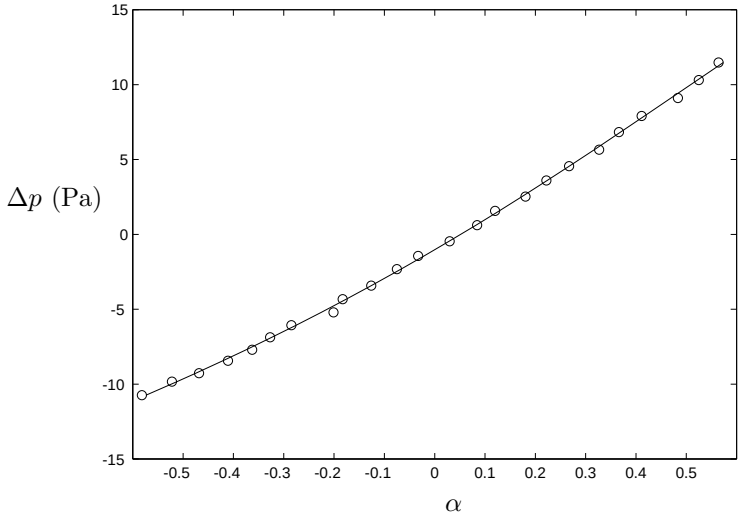

FIGURE 6. A typical calibration of a flow angle probe. The circles are measured points and the solid line is the fitted curve.

Most results are presented as contour plots with solid lines indicating positive values and dashed lines negative values. These figures are orientated so that the flow is into the paper sheet, *i.e.* we are looking in the downstream direction.

In measurements of this kind with very low fluctuations and very small mean variations it is very difficult to achieve accurate absolute and relative measures. This is partly because of the limitations in accuracy and resolution of the instrumentation such as pressure transducers, anemometers, multimeters and sensors. Measurement noise problems associated with high gains are also encountered. The accuracy of the location of the contours in the figures presented below are varying slightly between repeated measurements but the trends and the average values given in the figures were found to be the same.

3.1. *Total pressure measurement*

The total pressure variation over the cross section area of the test section is a good measure of the mean velocity variation. A variation of *e.g.* 0.1 % in total pressure corresponds to a variation of 0.05 % in streamwise velocity. From the total pressure in the test section, p_{test}, the total pressure in the stagnation chamber, p_{stag}, is subtracted to form the pressure difference measured by the differential pressure transducer in the experiments. The measured pressure is then divided by the dynamic pressure at the center of the measurement area, q_{test}, to form the dimensionless measure of the total pressure variation,

$$\frac{\Delta p_{\text{test}}(y,z)}{q_{\text{test}}} = \frac{p_{\text{test}}(y,z) - p_{\text{stag}}}{q_{\text{test}}} \tag{11}$$

where y and z are the vertical and horizontal directions.

The variation in total pressure was measured at three different test section velocities, 10 m/s, 25 m/s and 40 m/s. The results are shown in figure 7 with dashed lines corresponding to negative values and solid lines positive values.

At a test section speed of 10 m/s, (figure 7a), the variation of the total pressure is less than $\pm 0.10\%$. All contour curves here represent negative values contrasting with figures corresponding for the higher free-stream velocities. One reason for this could be that the accuracy of the absolute pressure measured by the pressure transducer is not high enough resulting in a constant pressure error. Another reason might also be that the pressure-loss in the contraction is relatively speaking higher in this case than at the other test section velocities. This is however contradicted by the fact that there is more positive contours for the 25 m/s case (figure 7b) than at the 40 m/s case (figure 7c).

At a test section speed of 25 m/s, (figure 7b), the variation in total pressure is less than $\pm 0.06\%$ over the measurement region. Note that the total pressure is higher in the left hand side and lower in the right hand side of the figure indicating that there is a velocity gradient in the horizontal direction over the cross section area. Although the gradient is small it is seen in repeated measurements. The maximum variation in total pressure variation is well within the expected limits.

At a test section speed of 40 m/s, (figure 7c), the variation in total pressure is very similar but slightly higher than for the 25 m/s case with a maximum variation of $\pm 0.09\%$. The gradient in the horizontal direction found for the 25 m/s case is also found at 40 m/s.

The overall results for the total pressure variation is very good with a maximum variation of less than $\pm 0.1\%$ over the velocity range studied. The results compare well with the findings in Johansson (1992) where the maximum variation was reported to be less than $\pm 0.1\%$. The flow uniformity does not seem to have been affected in a negative way by the 10 years of operation of the wind-tunnel.

3.2. *Temperature measurement*

The variation of temperature in the test section is of importance when temperature sensitive measurement techniques, such as hot-wire and hot-film anemometry, are used. The temperature in the MTL wind-tunnel varies with the same order of magnitude in both time and space. Long measurement times were used at each point in space for good averages and several measurements under the same conditions were made to confirm the results. Although the position of

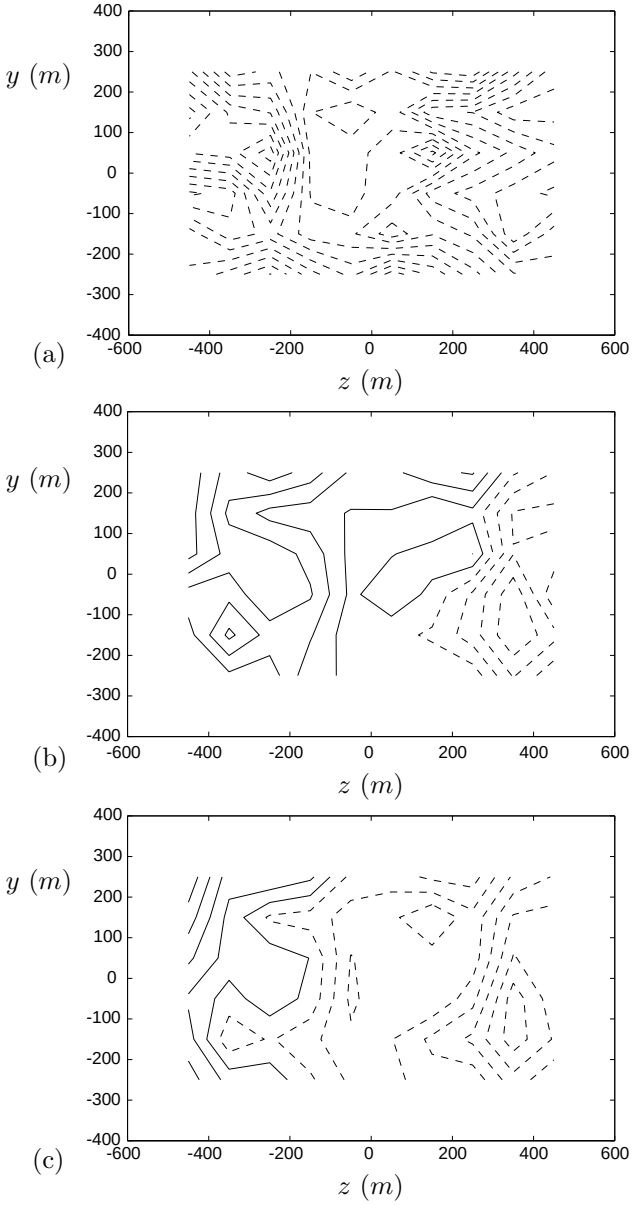

FIGURE 7. The total pressure variation over the cross section area of the test section at a free stream velocity of 10 m/s (top), 25 m/s (middle) and 40 m/s (bottom). Each line represents an increment of 0.01 % with dashed lines representing negative values and solid lines positive values.

each curve in the contour plots in figure 9 varies slightly between the measurements the trends are always similar confirming repeatability. The temperature contours presented in figure 9 are calculated as the temperature deviation from the mid-range value normalized by the mean temperature (in °C), i.e.

$$\Delta T = \frac{T(y,z) - \frac{1}{2}\left(T_{max}(y,z) + T_{min}(y,z)\right)}{\overline{T(y,z)}}, \tag{12}$$

where T is the temperature and y and z is the vertical and horizontal coordinates. The mid-range value is subtracted to give a clearer picture of the temperature variation in the figure. The mean temperature in the measurements is about 20 °C.

The temperature variation over the measurement area in the test section was measured at 10 m/s, 25 m/s and 40 m/s. The flow direction in the contour plots in figure 9 is into the paper sheet.

At 10 m/s the variation in temperature was less than ±0.2 % or ±0.04 °C, see figure 9a. This is a very small difference with the maximum temperature peak at about $z = -250$ mm and $y = 50$. This peak is also found at the other two tunnel speeds at a similar position. As was the case for the total pressure measurements the variation of the temperature over the cross section area at this low velocity differs from the higher velocity cases. The trend in figure 9 was confirmed by repeated measurements.

The variation in time is for the same test section velocity ±0.04 °C, see figure 8a. This variation is of the same magnitude as the variation over the cross section area. The variation in time has a typical period of 300 s sometimes interrupted by longer periods of more constant temperature. A hot-wire sampling time seldom exceeds 30 s which is one tenth of a period. A measurement can therefore occur at any time in the period. A hot-wire usually has a temperature of almost two hundred degrees making the errors small even between samples taken at times coinciding with the high and low extreme points in the temperature oscillation.

At a test section speed of 25 m/s the temperature variation in space over the measurement area was ±0.25 %, or ±0.05 °C see figure 9b. Here we find the peak also present in the 10 m/s case at $z = -350$ mm and $y = 50$. Furthermore, it can be seen that the upper right corner is cooler than the lower left corner. A possible reason could be that the cooling water enters in the top right corner and at the middle right side and that it exits at the lower right corner and the middle right side.

The variation in time over a period of 3 hours was ±0.05 °C, see figure 8b, which is slightly higher than at the test section velocity of 10 m/s. The higher temperature at the beginning in figure 8b is ignored because it is remains from the settling time of the cooling system. The period of the fluctuation is about 170 s which is almost half the period found at 10 m/s.

At the highest test section speed of 40 m/s the variation in space increased further to a value of ±0.35 %, see figure 9c, or ±0.07 °C. The pattern of variation is very similar to the one found at 25 m/s and the peak at $z = -350$ mm and $y = 50$ is still present.

The variation in time was about ±0.05 °C which is slightly higher than for the 25 m/s case, see figure 8c. The fluctuation period is here also 170 s. Overall the similarity between the 25 m/s and the 40 m/s cases are strong. One difference however is the increasing amplitude in the short time fluctuations seen as a thickening of the line with increasing speed in figure 8. This is caused by the slow response time of the cooling system and it is the result of too long piping between the heat exchangers and the constant flow rate of the cooling water.

Comparing with the first study by Johansson (1992), that found a temperature variation of ±0.2 °C, the variation has improved mainly due to a better system regulator. It is important to notice that the regulator, in this case, was not calibrated for each speed separately. This means that it probably is possible to get a slightly steadier temperature in time than what is presented here. However, the process of finding the best calibration constants for the regulator is rather time consuming. Therefore we did not do it here making our results a better representation for the temperature variations found in a typical MTL wind-tunnel experiment.

The settling time for the temperature, *i.e.* the time it takes to reach the desired temperature in the test section with minimum fluctuations in time from a new start of the wind-tunnel is fairly long. *E.g.* at a test section velocity of 25 m/s it takes approximately 30 minutes to stabilize the temperature. The reason for these long settling times is the simple type of regulator used at the moment in the tunnel, (PID) and the long piping between the regulator valve and the heat exchanger. There have been a discussion of improving this system in the future. A software based regulator with increased input information and improved piping is used in a newly built wind-tunnel at the department, see Lindgren & Johansson (2002), and it has the potential to shorten the settling time and decrease the temperature variation from the values found here in the MTL wind-tunnel.

3.3. *Flow angularity measurement*

The flow angularity is a measure of the straightness of the flow *i.e.* the ratio between the two cross flow velocities and the streamwise velocity. The flow angle is calculated by measuring the pressure difference of two symmetrically placed holes on a special probe, see section 2.2.3. By rotating the probe 90° both cross stream components, α in the vertical direction and β in the horizontal direction, could be measured at the same position. The mean flow angle was then subtracted from the measured values giving a relative measure of the

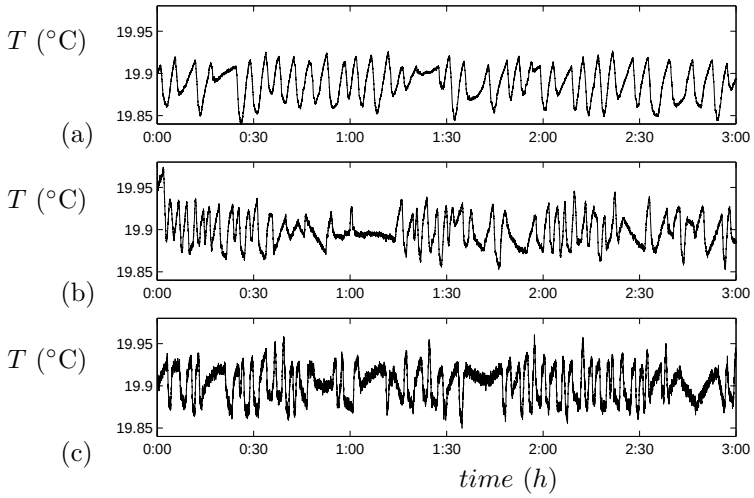

FIGURE 8. The temperature variation in time in the center of the test section cross section area at a free stream velocity of 10 m/s (top), 25 m/s (middle) and 40 m/s (bottom).

flow angularity. It is very difficult to exactly define which direction should give zero flow angularity since the test section walls are not completely parallel. Through the subtraction however we find important information on vortices and the flow pattern over the measurement area. The flow angularity is here defined as

$$\alpha(y,z) = \alpha_m(y,z) - \overline{\alpha_m(y,z)} \tag{13}$$

$$\beta(y,z) = \beta_m(y,z) - \overline{\beta_m(y,z)} \tag{14}$$

where the index m indicates measured values.

The flow angularity was measured at the three test section speeds 10 m/s, 25 m/s and 40 m/s. The pattern and magnitude of the arrows are similar at all three velocities indicating that the flow pattern is fairly independent of the velocity, see figure 10. The maximum magnitude of the arrows is about 0.25° at the edge of the measurement area and close to zero at the center. The measurements clearly reveals a flow pattern where the fluid expands from the center towards the test section walls.

Note that the probe was calibrated in the center of the test section with zero angularity in a direction that by eye sight was thought to be the mean flow direction. However, from the calibration curve, see figure 6, it can be seen that this direction does not represent zero pressure difference.

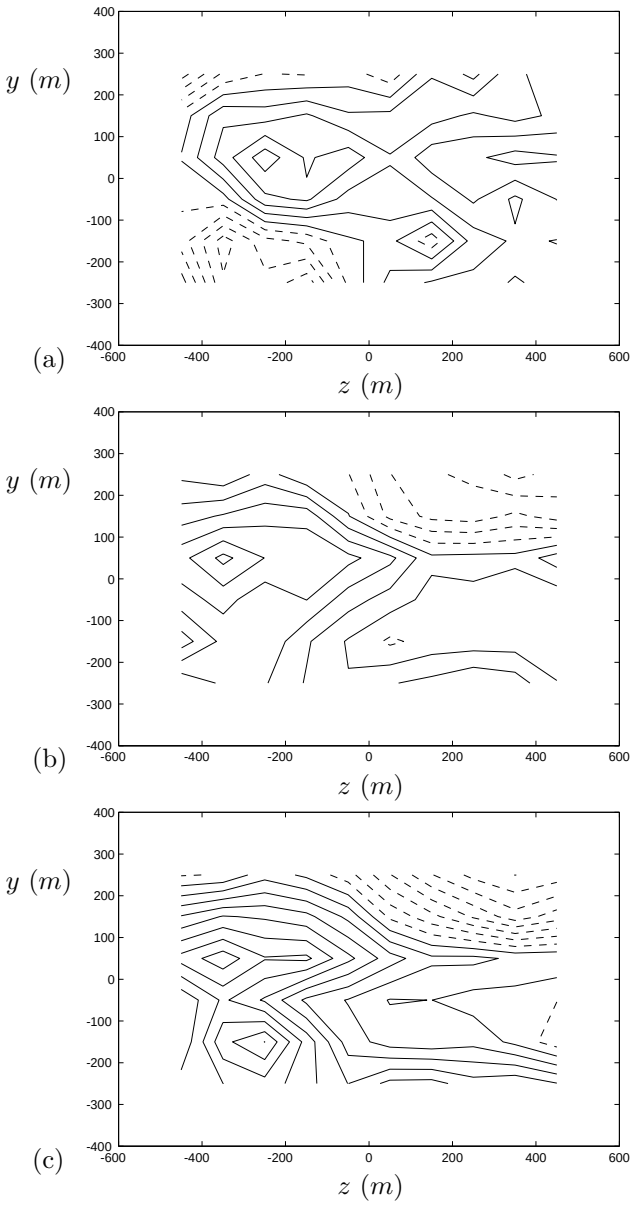

FIGURE 9. The temperature variation over the measurement area of the test section at a free stream velocity of 10 m/s (top), 25 m/s (middle) and 40 m/s (bottom). Each line represents an increment of 0.05 % with dashed lines representing negative values and solid lines positive values.

There are several possible reasons for this result. First there is an actual expansion of the width of the test section, equal to 5 mm in 500 mm length or 0.06°, at the streamwise position where the measurements were performed. However this is partly compensated for by the boundary layer growth which is between 1.4 mm and 1.8 mm on each wall in the velocity range used here. There is also a slight variation in the height of the test section since the upper and lower walls are adjustable to compensate for wall boundary layer growth making it difficult to position them absolutely parallel. The slit in the roof, allowing the traversing sword to enter the test section, is not sealed allowing air to exit the test section due to the positive pressure encountered over the slit.

Johansson (1992) encountered flow angularities well below 0.1°. This value is much lower than the ones found in this study. The main reason for the large increase in flow angularity is probably that the slit in the Johansson (1992) study was completely sealed. During our measurements we opted for an open slit since this is the case for most experiments taking place in the MTL wind-tunnel. The rather large expansion of the width of the test section, 5 mm from the inlet to the measurement position, has not been reported earlier and it will also contribute to an outwards directed flow. This expansion could be caused by swelling of the plywood test section walls as wood is a material that easily changes shape and size with *e.g.* moisture and temperature.

3.4. *Turbulence intensity measurement*

A very important aspect of wind-tunnel flow quality is the level of turbulence intensity in the test section. Low free stream turbulence levels are essential in transition related experiments where all flow disturbances should be created and controlled by the experimentalist. Also in other types of flow experiments the level of free stream turbulence could be of importance. The turbulence intensities in the three spatial directions are simply defined as

$$I_{\mathrm{x}} = \frac{u_{\mathrm{rms}}}{U}, \tag{15}$$

$$I_{\mathrm{y}} = \frac{v_{\mathrm{rms}}}{U}, \tag{16}$$

$$I_{\mathrm{z}} = \frac{w_{\mathrm{rms}}}{U}, \tag{17}$$

where the streamwise mean velocity, U, is used for normalization of the rms data.

When comparing the level of turbulence intensity from different wind-tunnel studies it is important to consider the amount of high-pass filtering of the data. Normally high-pass filters are applied to remove contributions to the turbulence intensity from low frequency waves traveling the wind-tunnel

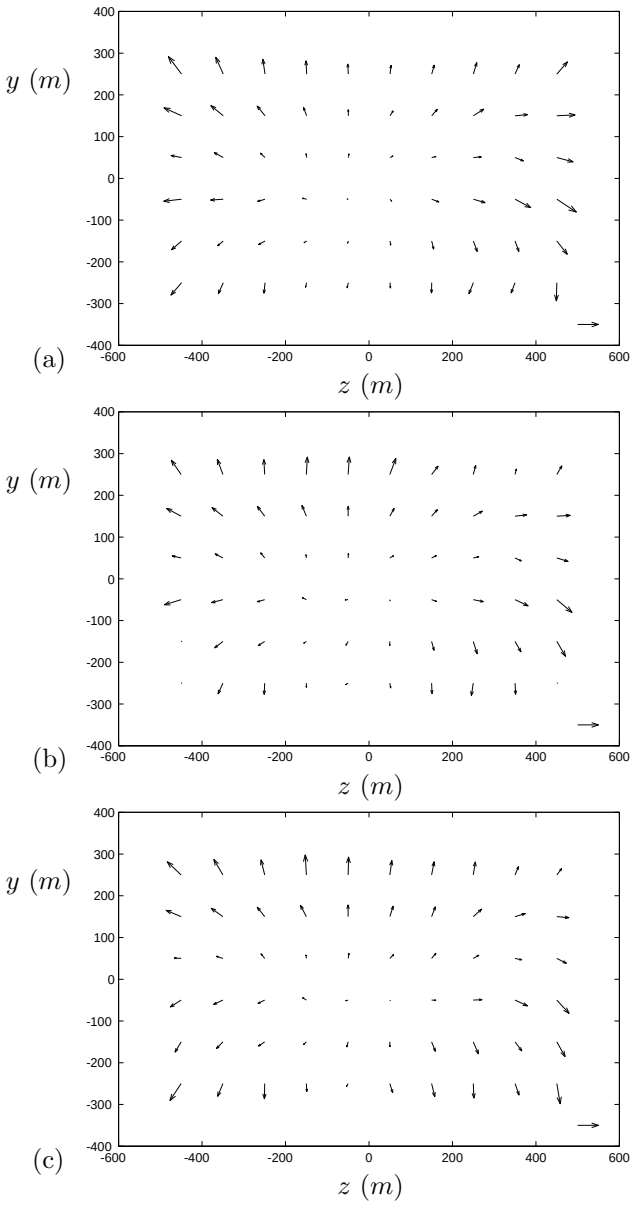

FIGURE 10. The cross flow direction over the cross section area of the test section at a free stream velocity of 10 m/s (top), 25 m/s (middle) and 40 m/s (bottom). The horizontal arrows at the lower right corner of the figures represents an angle of 0.25°.

circuit. The cut-off frequency is always chosen in a somewhat arbitrary manner. In this case we wanted all disturbances with wave lengths fitting in the test section cross section area to be conserved. Allowing for some margin we chose the wave length as the sum of the two test section side lengths, *i.e.* the cut-off wave length was chosen to be 2.0 m. A large part of the fluctuating energy is found at low frequencies which means that the filter can easily reduce the rms value by 50%. In this section the results will be provided for both unfiltered and high-pass filtered data. to simplify comparisons with results from other wind-tunnels and to visualize the impact of the filtering.

The cut-off frequency, f_c, is calculated from the free stream mean velocity, U and the cut-off wave length, λ_c as follows

$$f_c = \frac{U}{\lambda_c}. \tag{18}$$

The rms values are calculated by summation of the square of the absolute value of the Fourier coefficients from the time signal. The high-pass filtering is applied by summing only over the frequencies above the cut-off frequency. The rms values for the three velocity components thus read

$$u_{\mathrm{rms}} = \left(2 \sum_{k=N_c}^{N/2} |X_i|^2 \right)^{\frac{1}{2}}, \tag{19}$$

$$v_{\mathrm{rms}} = \left(2 \sum_{k=N_c}^{N/2} |Y_i|^2 \right)^{\frac{1}{2}}, \tag{20}$$

$$w_{\mathrm{rms}} = \left(2 \sum_{k=N_c}^{N/2} |Z_i|^2 \right)^{\frac{1}{2}}, \tag{21}$$

where X, Y and Z are the Fourier coefficients corresponding to the velocity time signals $u(x,y;t)-U(x,y)$, $v(x,y;t)-V(x,y)$ and $w(x,y;t)-W(x,y)$. N is the total number of samples and N_c is the summation index, k, corresponding to the frequency f_c.

The turbulence intensities were measured at the three different wind-tunnel speeds, 10 m/s, 25 m/s and 35 m/s. Note the change in velocity from 40 m/s to 35 m/s for the highest test section speed case compared to the previous results presented in this section. The reason for this is the influence from vibrations and acoustic noise from the probe holder devices at high speeds. The flow disturbances are very small and have much of their energy at low frequencies, typical also of vibrating stings, making it increasingly important to avoid these vibrations. The high-pass filtering could help removing vibrations. However,

there is no guarantee that these measurements are fully free from unwanted disturbances.

In the earlier study by Johansson (1992), measurements up to 60 m/s were obtained using another more rigid traversing arm. The increased flexibility and maneuverability of the traversing arm has here been exchanged with a lower maximum test section speed. The cut-off wave length in the Johansson (1992) study was 2.5 m which is slightly different from the one used in this study. This will have some effect on the results in the streamwise direction and less in the other two directions.

3.4.1. *Streamwise turbulence intensity results*

The streamwise turbulence intensity varies with tunnel speed being higher at low velocities.

At 10 m/s the level of turbulence intensity is less than 0.04% (figure 11a), when high-pass filtering is applied in the manner described above. The turbulence intensity is in general low over the measurement area but some increase can as expected be found towards the walls where the wall generated turbulence influences the results. These values are slightly higher than those found in the Johansson (1992) study, where the streamwise turbulence intensity was reported to be below 0.03% at all speeds between 5 m/s and 60 m/s. A ridge of slightly higher turbulence intensity is found just right of the vertical centerline in figure 11a. This ridge of unknown origin only appears at 10 m/s but can be found also for the two cross stream components. The total, unfiltered intensity is found to be less than 0.1% at 10 m/s (figure 11b) for this case.

At 25 m/s the streamwise turbulence intensity is less than 0.025% with higher values found towards the corners of the measurement region (figure 11c). This value compares well with the one found by Johansson (1992). The total unfiltered intensity is less than 0.08% (figure 11c).

At a tunnel speed of 35 m/s the streamwise turbulence intensity is less than 0.025%, see figure 11e. As in the 25 m/s case it is in one corner of the measurement area that the turbulence intensity exceeds 0.02%. At this velocity the results also compare well with the results found by Johansson (1992). The unfiltered intensity is less than 0.1%, see figure 11f, although it is very similar to the 25 m/s case in most of the measurement area except for one peak reaching above 0.08%.

As can be seen in the unfiltered data, (figures 11 b, d, f), the contours are not very smooth. The reason for this might be that the low frequency disturbances are not averaged over long enough time to give smoothly varying results. The sampling time of one minute at each point was set long enough to resolve the structures of the filtered signal.

No unfiltered data are available in the Johansson (1992) paper leaving us without comparisons here. However it seems that the unfiltered streamwise

turbulence intensity has increased somewhat over the years. This can be the result of dirt accumulation in honeycomb, screens and heat exchanger. Partly due to the increase in the usage of smoke recently for LDV, PIV and visualization measurements and to changes in fan blade angles for high pressure-loss experiments. After these measurements were completed it was found that there was an error in the manufacturing of the fan bearings leading to their destruction. The bearings have now been changed making the fan run more smoothly. A thorough cleaning of the tunnel and tuning of the fan blade angles would probably improve the unfiltered turbulence intensity results.

3.4.2. *Cross-stream turbulence intensity results*

The cross-stream turbulence intensities are expected to be slightly higher than the streamwise turbulence intensity because the damping of disturbances are much higher in the streamwise direction through the screens and contraction. This is also observed if only filtered data is considered. The low frequency disturbances related to the traveling waves in the wind-tunnel circuit appears only in the streamwise component and constitute a considerable contribution making the unfiltered streamwise turbulence intensity higher than its unfiltered cross flow counterparts. At low test section speeds (< 10 m/s) the filtered cross flow turbulence intensity is of the same magnitude as the streamwise turbulence intensity. At higher test section speeds the cross-flow components are slightly higher than the streamwise one.

At 10 m/s the filtered vertical and horizontal turbulence intensities are less than 0.04% and 0.05% respectively, see figures 12a and 13a. The vertical ridge slightly to right of the centerline found in the filtered streamwise case is also present for both the vertical and the horizontal turbulence intensities. For the unfiltered case, the cross-stream turbulence intensities are less than 0.05, see figures 12b and 13b. The effect of the high-pass filter is here almost negligible indicating that most disturbances are contained in higher frequencies than the cut-off frequency. This was expected from the reasoning above about low frequency traveling waves around the wind-tunnel circuit. An enlargement of the center region of very low turbulence intensity is the only difference between filtered and unfiltered data.

At 25 m/s the filtered vertical and horizontal turbulence intensities are less than 0.035% and 0.03% respectively, see figures 12c and 13c. The corresponding unfiltered values are both 0.04%, see figures 12d and 13d. Here, as for the 10 m/s case the difference between filtering and non-filtering is very small. Apart from the values in the corners the horizontal and vertical turbulence intensities are even lower than the numbers stated above.

At 35 m/s the filtered results for the vertical and horizontal turbulence intensity components are less than 0.04% and 0.03% respectively, see figures 12e and 13e. Their unfiltered counterparts are less than 0.04% and 0.05%, see

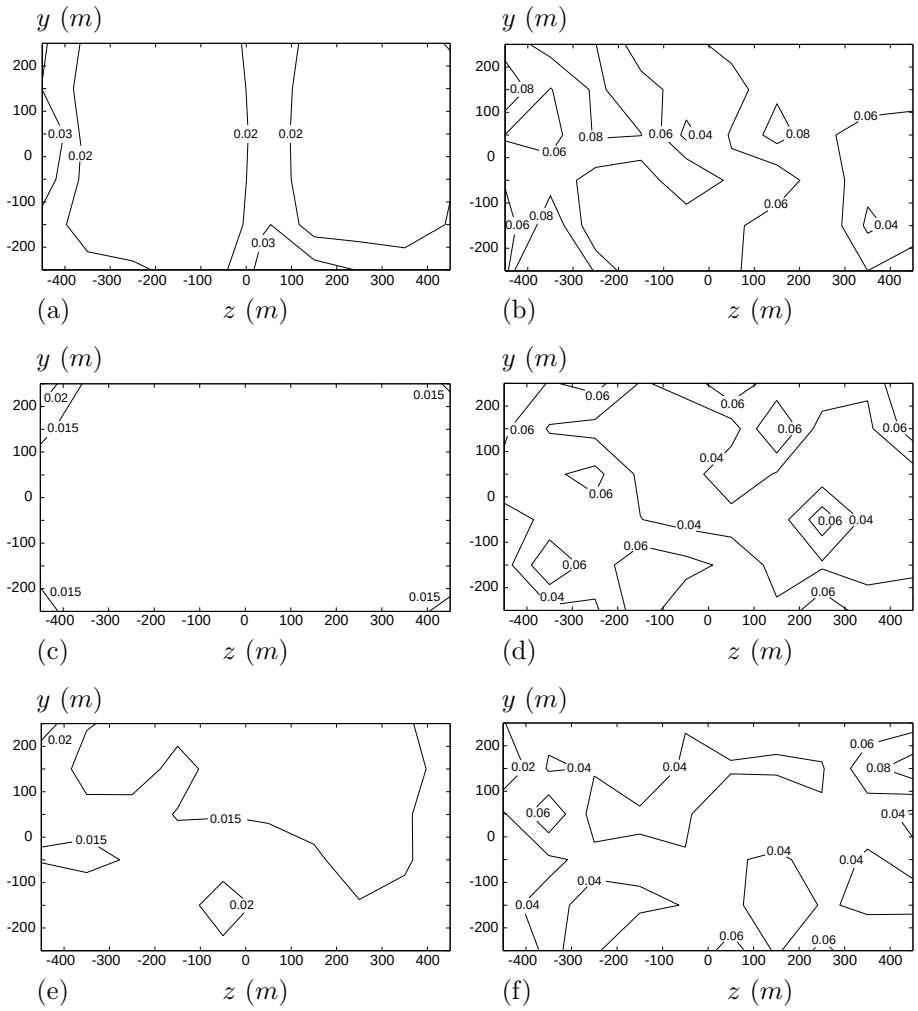

FIGURE 11. The streamwise turbulence intensity variation in % over the cross section area of the test section at a free stream velocity of 10 m/s (top), 25 m/s (middle) and 35 m/s (bottom). The left column represents the high pass filtered data with $U/f_c = 2.0$ m and the right column represents unfiltered data.

also figures 12f and 13f. The larger difference between filtered and unfiltered values for the horizontal component is the result of high unfiltered turbulence intensity in the upper left corner. Neglecting this corner reduces the difference to the values found for the other velocity cases.

In general the results for the cross flow turbulence intensities are well below the design criteria specified to the manufacturer of 0.09% also cited in Johansson (1992). There, the filtered cross-stream components were reported to be less than 0.06% in the velocity span of 5 to 60 m/s which is larger than the results presented here. The cross flow turbulence intensities increased also with increasing speed. This was not confirmed by this study where the cross flow turbulence intensities were more or less independent of test section speed. However the limited maximum velocity of 35 m/s used here is far from the 60 m/s maximum velocity reported by Johansson (1992) and the cross flow turbulence intensities might well increase with higher test section speeds.

The cross-stream turbulence intensity does not seem to have changed much over the years This is natural since wear on the driving unit and dirt deposition in screens etc mostly effects the pressure-loss and pressure waves which are directly related to the streamwise component.

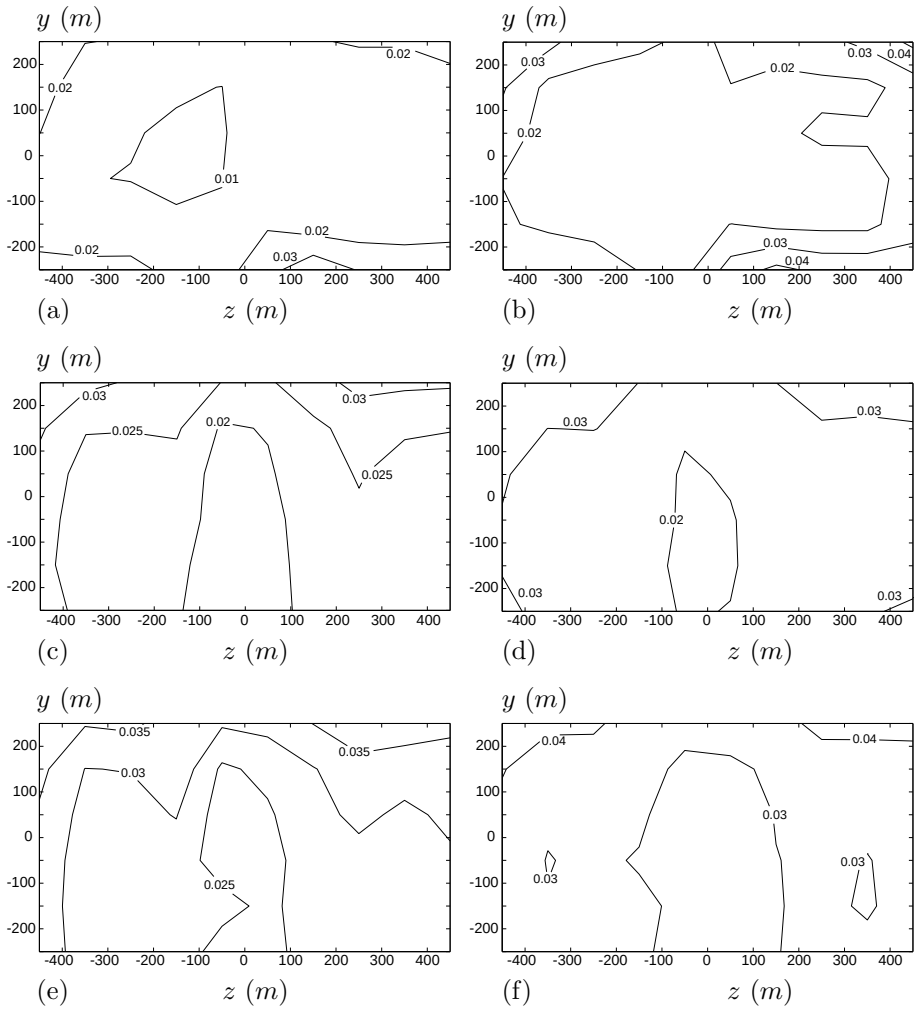

FIGURE 12. The vertical cross stream turbulence intensity variation over the cross section area of the test section at a free stream velocity of 10 m/s (top), 25 m/s (middle) and 35 m/s (bottom). The left column represents the high pass filtered data with $U/f_c = 2.0$ m and the right column represents unfiltered data.

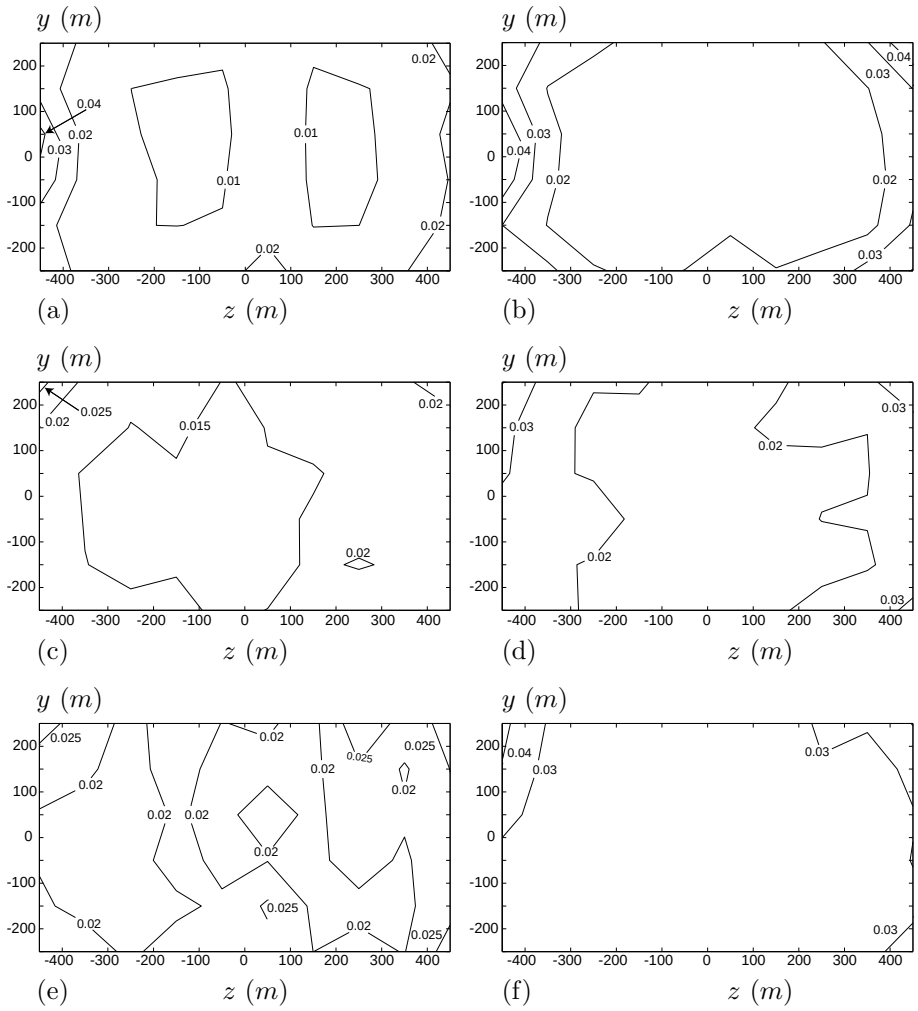

FIGURE 13. The horizontal cross stream turbulence intensity variation over the cross section area of the test section at a free stream velocity of 10 m/s (top), 25 m/s (middle) and 35 m/s (bottom). The left column represents the high pass filtered data with $U/f_c = 2.0$ m and the right column represents unfiltered data.

4. Concluding remarks

The flow quality in the MTL wind-tunnel at the Department of Mechanics, KTH has been investigated. It was also studied in connection with the construction of the wind-tunnel. The results from these early measurements are reported in Johansson (1992). The reason for performing new measurements were both to improve the documentation of the flow quality and to investigate how the flow quality has changed after 10 years of extensive use of the facility. In the new experiments the same quantities as in the early experiment have been measured except for static pressure variations over the test section measurement area. It was measured in the early experiment but left out here due to the high difficulty in achieving results not influenced by changes in dynamic pressure.

The total pressure variation over the test section cross section area is less than $\pm 0.06\%$ at a test section speed of 25 m/s and slightly larger at 10 m/s and 40 m/s. These results are well in line with those found earlier by Johansson (1992) that reported a total pressure variation of less than $\pm 0.1\%$ over a test section velocity range of 5 to 60 m/s. The variation in total pressure variation has not been severely effected by time.

The temperature variation over the measurement area was found to be less than $\pm 0.05\ ^{\circ}C$, (at 25 m/s), which is substantially smaller than the initial findings by Johansson (1992) of $\pm 0.2\ ^{\circ}C$, due to a better control of the cooling system.

The temporal variation of the temperature is less than $\pm 0.04^{\circ}C$ at a test section speed of 10 m/s and $\pm 0.05^{\circ}C$ at test section speeds of 25 m/s and 40 m/s. The temperature variation in time is thus similar to the variation in space.

The flow angularity was measured over the measurement area using a special probe that is very sensitive to a change in position of the stagnation point. The results show a maximum deviation of 0.25° at the edges of the measurement area at all test section velocities. The flow is directed outwards towards the test section walls around the measurement area edge. The reason for this outwards directed flow is an increase in the cross section area of the test section in the vicinity of the downstream measurement position, partly compensated for by boundary layer growth, and the unsealed slit in the upper wall allowing air to flow out from the test section where the static pressure is slightly larger than the atmospheric pressure outside. A comparison with the earlier measurements by Johansson (1992) shows that the flow angle variation observed in the present investigation is substantially larger, partly because of the introduction of the traversing system. The maximum flow angularity was in the early study below 0.1°.

The turbulence intensity has been measured in the streamwise and the vertical and horizontal cross-stream directions. At a test section velocity of 25

m/s the streamwise turbulence intensity was found to be less than 0.025% and the vertical and horizontal cross-stream turbulence intensity components was less than 0.035% and 0.03% respectively. Here, the data was high-pass filtered removing structures with wave lengths longer than 2.0 m. At the other speeds investigated (10 and 35 m/s) the intensities were found to be somewhat higher.

These results compares well with those found by Johansson (1992) and they are within the original design criteria. The unfiltered streamwise turbulence intensity is higher than what was expected but it can probably be lowered by adjusting the fan blade angles and cleaning the wind-tunnel screens, guide vanes and heat exchanger.

In general the MTL wind-tunnel still has an overall flow quality to well justify the name, Minimum Turbulence Level. Some deterioration has been noticed mainly in flow angularity and unfiltered turbulence levels. These problems are though thought to be of such nature that a minor overhaul could well be enough to restore the initial performance. The general flow quality indicates a good potential for the MTL wind-tunnel to be a high-quality tool in transition and turbulence research also for the coming ten years. The increased use of optical measurement methods, such as LDV and PIV requiring seeding, implies an increased need for regular cleaning of the interior of the tunnel.

5. Acknowledgment

The authors would like to thank Valeria Durañona from the Technical University of Uruguay, Montevideo, Uruguay, for assistance in some of the measurements. Further thanks goes to Ulf Landén for his aid in manufacturing the measurement equipment. Henrik Alfredsson is greatfully acknowledged for many comments on the manuscript and for sharing the main responsibility of the planning and design of the MTL wind-tunnel with the second author. Finally financial support from the Swedish Research Council for the first author is greatfully acknowledged.

References

Baines, W. & Peterson, E. 1951 An investigation of flow through screens. *Trans. ASME* **73**, 467–480.

Boiko, A. V., Westin, K. J. A., Klingmann, B. G. B., Kozlov, V. V. & Alfredsson, P. H. 1994 Experiments in a boundary layer subjected to free-stream turbulence. part 2. the role of TS-waves in the transition process. *J. Fluid Mech* **281**, 219–245.

Borger, G. G. 1976 The optimization of wind tunnel contractions for the subsonic range. *Tech. Rep.* TTF 16899. NASA.

Downie, J. H., Jordinson, R. & Barnes, F. H. 1984 On the design of three-dimensional wind tunnel contractions. *J. Royal Aeronautical Society* pp. 287–295.

Elofsson, P. A. & Alfredsson, P. H. 1998 An experimental study of oblique transition in plane poiseuille flow. *J. Fluid Mech* **358**, 177–202.

Groth, J. & Johansson, A. V. 1988 Turbulence reduction by screens. *J. Fluid Mech* **197**, 139–155.

Häggmark, C. P., Bakchinov, A. A. & Alfredsson, P. H. 2000 Experiments on a two-dimensional laminar separation bubble. *Phil. Trans. R. Soc. Lond. A* **28**.

Johansson, A. V. 1992 A low speed wind-tunnel with extreme flow quality-design and tests. *Proc. the 18:th ICAS Congress* pp. 1603–1611.

Johansson, A. V. & Alfredsson, P. H. 1988 *Experimentella metoder i strömningsmekaniken*. Department of Mechanics, Royal Institute of Technology.

Laws, E. & Livesey, J. 1978 Flow through screens. *Ann rev Fluid Mech.* **10**, 247–266.

Lin, J. C., Selby, G. V. & Howard, F. G. 1991 Exploratory study of vortex-generating devices for turbulent flow separation control. In *29th AIAA Aerospace Sciences Meeting, Reno, Nevada*. AIAA paper 91-0042.

Lindgren, B. & Johansson, A. V. 2002 Design and calibration of a low-speed wind-tunnel with expanding corners. TRITA-MEK 2002:14. Department of Mechanics, KTH.

Loehrke, R. I. & Nagib, H. M. 1976 Control of free-stream turbulence by means of honeycombs: A balence between suppression and generation. *J. Fluids Engineering* pp. 342–353.

Lumley, J. L. 1964 Passage of turbulent stream through honeycombs of large length-to-diameter ratio. *Trans. ASME, J. Basic Engineering* **86**, 218–220.

Matsubara, M. & Alfredsson, P. H. 2001 Disturbance growth in boundary layers subjected to free stream turbulence. *J. Fluid Mech.* **430**, 149–168.

Mikhail, M. N. & Rainbird, W. J. 1978 Optimum design of wind tunnel contractions, paper 78-819. In *AIAA 10th Aerodynamic Testing Conference*.

Österlund, J. M. 1999 Experimental studies of zero pressure-gradient turbulent boundary-layer flow. PhD thesis, Department of Mechanics, Royal Institute of Technology, Stockholm.

Österlund, J. M. & Johansson, A. V. 1999 Turbulent boundary layer experiments in the MTL wind-tunnel. TRITA-MEK 1999:16. Department of Mechanics, KTH.

Österlund, J. M., Johansson, A. V., Nagib, H. M. & Hites, M. H. 2000 A note on the overlap region in turbulent boundary layers. *Phys. Fluids* **12**, 1–4.

Sahlin, A. & Johansson, A. V. 1991 Design of guide vanes for minimizing the pressure loss in sharp bends. *Phys. Fluids A* **3**, 1934–1940.

Scheiman, J. & Brooks, J. D. 1981 Comparison of experimental and theoretical turbulence reduction from screens, honeycomb and honeycomb-screen combinations. *JAS* **18**, 638–643.

Seidel, M. 1982 Construction 1976-1980. design, manufacturing, calibration of the

German-Dutch wind tunnel (DNW). *Tech. Rep.*. Duits-Nederlandese Windtunnel (DNW).

Sjögren, T. & Johansson, A. V. 1998 Measurement and modelling of homogeneous axisymmetric turbulence. *J. Fluid Mech* **374**, 59–90.

Tan-Atichat, J., Nagib, H. M. & Loehrke, R. I. 1982 Interaction of free-stream turbulence with screens and grids: a balance between tubulence scales. *J. Fluid Mech.* **114**, 501–528.

Taylor, G. & Batchelor, G. K. 1949 The effect of wire gauze on small disturbances in a uniform stream. *Quart. J. Mech. and App. Math.* **2**, part 1,1.

Westin, K. J. A., Boiko, A. V., Klingmann, B. G. B., Kozlov, V. V. & Alfredsson, P. H. 1994 Experiments in a boundary layer subjected to free-stream turbulence. Part 1. Boundary layer structure and receptivity. *J. Fluid Mech* **281**, 193–218.

Wikström, P. M., Hallbäck, M. & Johansson, A. V. 1998 Measurements and heat-flux transport modelling in a heated cylinder wake. *Int. J. Heat and Fluid Flow* **19**, 556–562.

Appendix

Here follows a list of the Doctoral and Licentiate theses so far produced at the Department of Mechanics, KTH, where experiments performed in the MTL wind-tunnel are included. There is also a list of selected papers, not included in a thesis, based on experiments in the MTL tunnel.

Doctoral theses in chronological order

1. JOHAN GROTH, On the modeling of homogeneous turbulence, 1991, ISRN KTH/MEK/TR–91/00–SE.
   Groth's thesis includes work on screen turbulence which was used in determining the size and number of screens to have in the MTL wind-tunnel. These results are also published in Groth & Johansson (1988).
2. TORBJÖRN SJÖGREN, Development and calibration of turbulence models through experiment and computation, 1997,
   ISRN KTH/MEK/TR–97/05–SE.
   Torbjörn Sjögren performed the first experiment where the pressure-strain rate term in (statistically) axisymmetric turbulence was directly measured. These results are also presented in Sjögren & Johansson (1998).
3. JOHAN WESTIN, Laminar turbulent boundary layer transition influenced by free stream turbulence, 1997,
   ISRN KTH/MEK/TR–97/10–SE.
   Results concerning non-parallel effects on boundary-layer stability were found and these results are reported in Westin *et al.* (1994) and Boiko *et al.* (1994).
4. PER ELOFSSON, Experiments on oblique transition in wall bounded shear flows, 1998, ISRN KTH/MEK/TR–98/05–SE.
   Per Elofsson made investigations of the role of oblique transition in Poiseuille and Blasius flows which are reported in Elofsson & Alfredsson (1998).
5. PETRA WIKSTRÖM, Measurements, direct numerical simulation and modeling of passive scalar transport in turbulent flows, 1998,
   ISRN KTH/MEK/TR–98/11–SE.
   Experiments on passive scalars (temperature) in a cylinder wake were performed. Special care was taken to measure the Reynolds fluxes. See also Wikström *et al.* (1998).
6. JENS ÖSTERLUND, Experimental studies of zero pressure-gradient turbulent boundary layer flow, 1999, ISRN KTH/MEK/TR–99/16–SE.
   Jens Österlund established the log-law for z.p.g. turbulent boundary layer flow and determined new values for the Kármán and additive constants. These findings are reported in Österlund *et al.* (2000).

7. CARL HÄGGMARK, Investigations of disturbances developing in a laminar separation bubble flow, 2000,
   ISRN KTH/MEK/TR–00/03–SE.
   Investigations were made on highly instable high frequency two-dimensional waves in a laminar separation bubble, see Häggmark *et al.* (2000).

Licentiate theses in chronological order

1. KRISTIAN ANGELE, PIV measurements in a separating turbulent APG boundary layer, 2000, ISRN KTH/MEK/TR–00/15–SE.
   This work focuses on scaling and structures of in a turbulent separation bubble.
2. JENS FRANSSON, Investigations of the asymptotic suction boundary layer, 2001, ISRN KTH/MEK/TR–01/11–SE.
   This work is mainly focused on the study of the asymptotic suction boundary layer.

Selected papers in chronological order

Other papers, not included in a thesis from the Department of Mechanics, involving measurements in the MTL wind-tunnel are listed below.

1. Sahlin & Johansson (1991)
   Alexander Sahlin was part of the MTL aerodynamic design team. Among other things he developed the guide-vanes used in the present tunnel. He was also heavily involved in the calibration of the wind-tunnel.
2. Matsubara & Alfredsson (2001)
   Matsubara has made experiments on instabilities and their growth in laminar boundary layers. Some of which are reported in the above cited paper.

Ongoing theses/post doc work

There are still work in process in the MTL wind-tunnel that will be published in the future. In the list below, the people currently involved in measurements in the MTL wind-tunnel, are listed in alphabetical order.

1. Kristian Angele, (Dr. thesis work)
   Title: Turbulent flow separation.
2. Jens H. M. Fransson, (Dr. thesis work)
   Title: Investigations of the asymptotic suction boundary layer.
3. Björn Lindgren, (Dr. thesis work)
   Title: Flow facility design and experimental studies of wall bounded turbulent shear-flows
4. Fredrik Lundell, (Dr. thesis work)
   Title: An experimental study of by-pass transition and its control.

5. Davide Medici, (Dr. thesis work)
   Title: Non-axisymmetric wakes and the possibility to optimize the power output of wind-turbine farms.
6. Shuya Yoshioka, (Post. Doc. work)
   Title: Boundary layer suction for reduction of friction drag.